Interfacial symmetry-breaking effects in the quantum paraelectric $SrTiO_3$

Hang-Bo Zhang,[1] Marin Alexe[1*]

[1] *Department of Physics, University of Warwick, Coventry CV4 7AL, UK*

[*]Email: m.alexe@warwick.ac.uk

ABSTRACT

Oxides lacking a centre of symmetry, are highly desired as they usually bring in fascinating physical properties. However, there are limited numbers of non-centrosymmetric media in nature and most of them do not have multiple functionalities integrated. Here, using the bulk photovoltaic effect as the probing technique, we demonstrate that at interfaces with a wide range of oxides strontium titanate ($SrTiO_3$) is polar, i.e., with broken inversion symmetry in the quantum paraelectric phase. Studies comprising conductivity and bulk photovoltaic effect on $LaAlO_3/SrTiO_3$ thin films further show excessive electronic band bending screens the induced polarity, revealing that an appropriate band bending at the interface is the key parameter to control the symmetry breaking. Inheriting the high carrier mobility from $SrTiO_3$, the polar interface under illumination at low temperatures is conductive or metallic, permitting the multifunctionality coupling between the oxides and $SrTiO_3$. Our studies show that significant photovoltaic effects can be generated at the polar interfaces especially in the quantum-paraelectric phase of $SrTiO_3$, giving thus practical design strategies for multi-functional devices.

I. INTRODUCTION

$SrTiO_3$ (STO) and its heterostructures with dissimilar materials are proven to show fascinating physical functionalities, especially in the low-temperature regime. The ultrahigh dielectric constant [1,2], two-dimensional electron gas (2DEG) [3,4], and superconductivity [5,6] are only a few emerging properties usually associated with either high carrier mobility [7] or the quantum paraelectric phase [8,9] of STO. The quantum paraelectricity, where the quantum fluctuations between degenerate lower symmetry configurations suppress ferroelectric ordering [2], can be further induced into a polar state by an external field [9] or chemical substitution [10,11], enriching the functionality of the system or even coupling ferroelectricity/ferromagnetism and superconductivity [12,13]. All these interesting properties made STO one of the most popular materials for oxide electronics [14].

As recently highlighted, a band bending at a metal-oxide (Schottky) junction is inherently associated with a built-in electric field [15], that breaks the inversion symmetry at the interface. This is, in principle, not a characteristic of a metal-semiconductor interface. A built-in electric field commonly exists at the interface of any two dissimilar materials (e.g., metal-semiconductor, semiconductor-semiconductor) due to a generic band bending needed to align the Fermi level across the interface [16,17]. For STO, a polar interface might be easily induced at the quantum paraelectric phase regime.

We show here that many oxide-STO heterostructures have polar interfaces in the quantum paraelectric regime of STO, detected by a bulk photovoltaic effect that only exists in the non-centrosymmetric media. Further, we demonstrate that the magnitude of the polarity of the interface can be tuned in the $LaAlO_3$-$SrTiO_3$ (LAO/STO) system by fabrication conditions. These properties along with the well-known high carrier mobility of STO could bring unexpected properties, such as metallic ferroelectricity [18].

II. EXPERIMENTS

A. Synthesis of $SrTiO_3$-based heterostructures

TiO_2-terminated (001)-oriented $SrTiO_3$ substrates were by etching in buffered HF for 15 s and then annealed in the air at 1200 ℃ for 2 h. LAO/STO thin films were grown by pulsed laser deposition (PLD) at 10^{-3} mbar oxygen pressure. The laser energy density was 1 J/cm^2 and the repetition rate was 2 Hz. Samples LAO/STO #1, #2, #3 and #4 were grown at 600 ℃, 650 ℃, 700 ℃ and 750 ℃, respectively. LAO thin film thickness was in all cases ~10 nm. The growth of ~50 nm thick Fe_2O_3 thin films were deposited on STO by PLD at 10^{-5} mbar and 600 °C with a laser fluence of 0.5 J/cm^2 and a repetition rate of 5 Hz. 40 nm Au and 20 nm Al were evaporated on the surface of $SrTiO_3$ to fabricate Au/STO and Al/STO, respectively.

B. Electrical measurements

The homemade optical PPMS insert was used for 10-300 K temperature-dependent measurement. A polarised 405 nm laser (40 mW nominal power, Thorlabs, DL5146-101S) was used to generate linearly polarised light. The light polarization direction was rotated at a rate of 2 degrees per second using a half-wave plate (Thorlabs, model AHWP05M-340) (HWP). A high impedance electrometer (Keithley 6517B) was used to collect the time-dependent photocurrent, i.e., wave plate angle-dependent photocurrent. An AixACCT TF3000 ferroelectric workstation was employed to study the ferroelectric polarization switching behavior in our work. For each electrical measurement, we stabilised the system for sufficient time until current drift effect or light-induced heat vanished. (See detail in Fig. 6 of Appendix)

III. RESULTS

A. Characterization of the general symmetry breaking

Several oxide layers, as well as noble metals (Au), have been deposited on the (100) surface of (100)-oriented STO single crystals to induce the band-bending at the interface. The light polarization-dependent bulk photovoltaic (BPV) effect was used to probe the interface symmetry breaking underneath the capping layer [19] as the BPV effect only exists in the non-centrosymmetric media. If the innate centrosymmetry of the crystal is lifted and becomes polar. As a consequence, a BPV current will be generated by light penetrating the capping layer [20]. As a proof-of-concept experiment, the BPV current was firstly measured on a metal-semiconductor junction (Schottky) fabricated depositing a high work function metal that usually generated a large band bending within STO. As expected, the Au/STO system shows at room temperature a textbook linear BPV effect, indicating a symmetry breaking at the interface by simply contacting gold with the centrosymmetric STO crystal [15,20]. Fig. 1(b) shows the variation of photovoltaic (PV) current with respect to the relative angle between light polarization and crystallographic direction of the PV current, which is the fingerprint of the linear BPV (LBPV) effect. This angle is set using a half-wave plate (HWP), therefore from now, it will be denominated as HWP angle θ. According to the phenomenological theory [20,21], the LBPV current as a function of the HWP angle is expressed as:

$$J^{HWP} = J_L \sin(4(\theta + \theta^{off})) + J_L^{off} \quad (1)$$

where J_L is the amplitude LBPV current, θ^{off} is the LBPV angle offset and J_L^{off} is the LBPV current offset that is independent of the HWP angle. By least-square fitting the HWP angle-dependent photocurrent (as in Fig. 1(b)), we obtained the amplitude of the LBPV current and used it to characterise the LBPV effect.

To characterise the BPV effect in the quantum paraelectric regime of STO one needs to lower the temperature under a characteristic transition temperature of ~37 K and simultaneously measure the PV current. For this purpose, a physical property measurement system (PPMS)

with a homemade optical insert, schematically shown in Fig. 1(a), was used to characterise the optoelectrical properties from room temperature down to 10 K. The linearly polarised light modulated by a half-wave plate allows us to analyse the linear BPV current of the investigated samples [22].

As we decreased the temperature of the Au-STO, a remarkable increase of about three orders of magnitude of the photocurrent was observed below ~40 K (Fig. 1(c)). To exclude this LBPV response from the contribution of pristine STO bulk or surface, we ran similar experiments on STO with quasi-ohmic contacts, i.e., Aluminium. As expected, due to low work function, Al does not provide sufficient band bending at the Al/STO interface. Consequently, Al/STO does not show a BPV effect in the entire temperature range (see Fig. 1(c) and Fig. 4(b)). These results are consistent with the previous report that the metal-oxide Schottky junction can induce a polar structure at the interface while the ohmic contact cannot [15].

To investigate whether symmetry breaking also exists in oxide-STO interfaces, we firstly studied the LBPV effect in a Fe_2O_3/STO thin film. Neither of these materials should in principle show the BPV effect at any temperature. While this is true for high temperatures, by lowering the temperature under 40 K, a considerable LBPV response raises (Fig. 1(d)). Since both STO and Fe_2O_3 are centrosymmetric and normally do not show the BPV effect, their interface must be the origin of this giant LBPV response. We have assumed that this might be a generic effect in which bringing STO into the quantum paraelectric state, respectively lowering its temperature under transition temperature is an important ingredient. We further investigated the LBPV effect in the LAO/STO heterostructures, as being one of the iconic STO-based interfaces that have been massively investigated in the recent past [3,5].

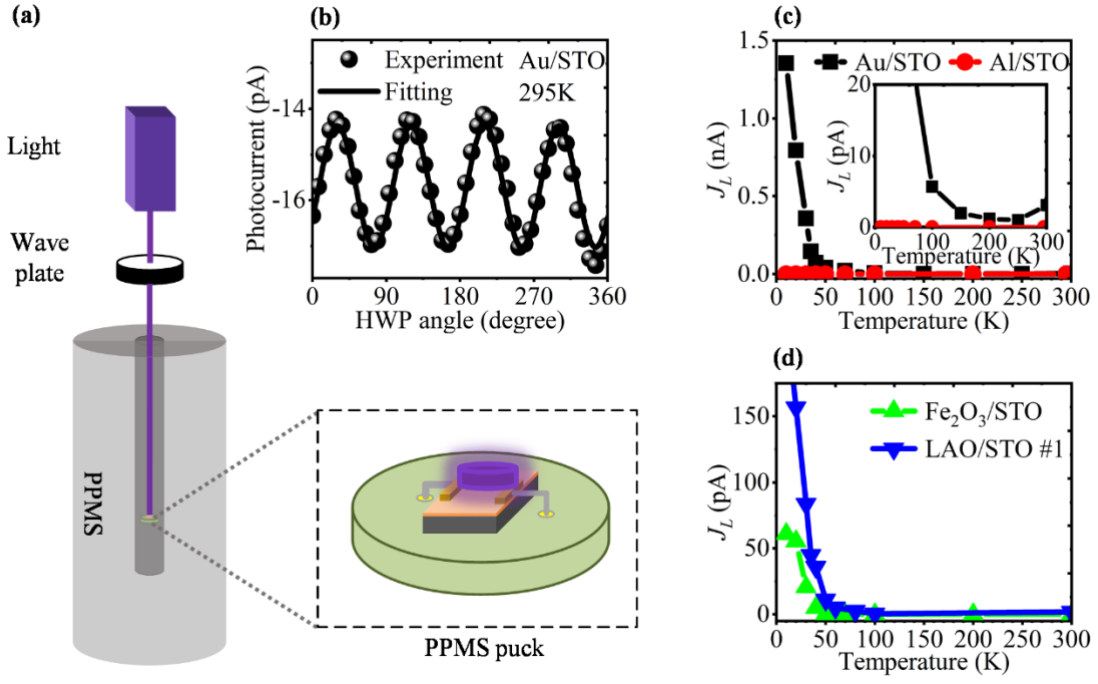

FIG. 1. Detection of general symmetry breaking of STO-based heterostructures via linear BPV effect. (a) schematic of the homemade optical PPMS. (b) HWP angle-dependent photocurrent of simple Au/STO junction at room temperature. (c) Temperature-dependent LBPV current amplitudes of Schottky contact Au/STO and quasi-ohmic contact Al/STO. The inset is the enlarged view of LBPV current amplitudes. (d) Temperature-dependent LBPV current amplitudes of Fe_2O_3/STO and LAO/STO #1.

Knowing that the electronic characteristics of this system are very sensitive to the growth conditions [23,24], we fabricate heterostructures depositing LAO thin films on STO at the

specific condition in which the 2DEG state is not yet formed, i.e., LAO/STO #1 thin film in our experiment (Fig. 2(b)). Similarly, to the Au/STO system, LAO/STO #1 has a weak BPV response at room temperature which increases several orders of magnitude below 40 K, as shown in Fig. 1(d) and Fig. 4(d).

The onset temperature of the massive LBPV response is about 40 K, close to the temperature of the emergence of the quantum paraelectric phase (37 K) in STO [9]. However, the nonpolar quantum paraelectric state is centrosymmetric and should in principle not show any BPV effect. The experimental evidence points us to the fact that this quantum paraelectric phase is in an ordered polar phase at the interface. It is well known that at the interface of any heterostructures based on two dissimilar materials a built-in voltage V_{bi} exists as a result of the band alignment to maintain the Fermi energy level flat across the interface [17] (e.g., LAO/STO system shown in Fig. 2(a)). This band bending results in a built-in electric field E_{bi} normal to the interface and forms a polar interface [15].

B. The tuneable polarity of the interface of the LAO-STO system

Next, we explore whether this polarity of the interface can be tuned or controlled through the fabrication process. Therefore, we focus on the well-studied LAO-STO heterostructures. It is known that the band bending in STO induces either a conductive or insulating interface, depending upon the position of the Fermi level with respect to the conduction band [17,25,26]. For example, if the conduction band at the interface is bent well below the Fermi level, a large density of available states becomes available, and the carriers may become mobile at the interface (Fig. 2(a)). It is known that oxygen vacancies are playing a key role in providing free electrons and tuning the interface conductivity [27,28]. In order to clarify the effect of the electronic reconstruction on the polarity of the interface, as they share the same influence from the interfacial band bending, we investigate the BPV effect and conductivity of a series of LAO/STO thin films with different interface doping densities. The latter is tuned by simply controlling the growth temperature of LAO thin films on STO substrate [29,30] (see Experiments section).

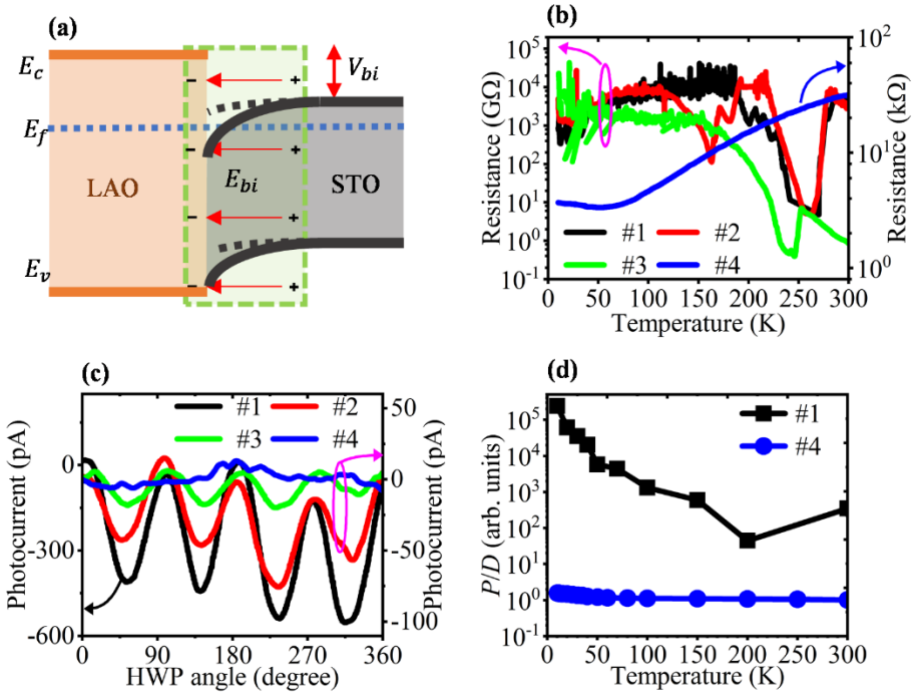

FIG. 2. The LBPV effect and conductivity characterizations of LAO/STO thin films grown at different temperatures. Samples #1, #2, #3, and #4 were grown at 600 ℃, 650 ℃, 700 ℃ and 750 ℃, respectively. (a) Illustration of the band-bending at the interface of LAO/STO. V_{bi} is the built-in voltage and E_{bi} is the built-in electric field. E_c, E_v and E_f are the conduction band, valence band and Fermi level, respectively. (b) temperature-dependent dark resistance of LAO/STO grown at different temperatures. Below 200 K, the dark current measurements of LAO/STO #1, #2 and #3 were limited by the current sensitivity as the dark resistance is very high. (c) HWP angle-dependent linear photovoltaic currents at 10 K of LAO/STO grown at different temperatures. (d) The ratio photoconductivity/dark conductivity (P/D) of LAO/STO #1 and #4 as a function of temperature.

The temperature-dependent dark resistance measurements (Fig. 2(b)) confirmed that the growth temperature can effectively tune the interface carrier density. Only the LAO/STO grown at 750 ℃ (LAO/STO #4) shows typical 2DEG temperature dependence of resistance, as previously reported [31]. Samples grown at lower temperatures show much higher resistance and non-2DEG-like temperature dependence (Fig. 2(b)). Further on, we studied the relationship between the LBPV currents and growth temperature. Interestingly, the LBPV response is opposite to the resistance behavior in the LAO/STO system. The LBPV current of LAO/STO thin film grown at the lowest temperature 600 ℃ (LAO/STO #1) is at least one order of magnitude higher than that measured on samples grown at higher temperatures. The presence of the LBPV effect indicates that symmetry breaking at the LAO/STO interface and implicitly the polar nature of the interface is stronger in LAO/STO #1 compared to all other samples. Noticeable, the LAO/STO grown at 750 ℃ (LAO/STO #4) showing 2DEG behavior does not exhibit any LBPV response.

The disjunction between the 2DEG and LBPV effects in LAO/STO reveals an apparent screening-like effect. In the 2DEG state, the thermally activated carrier density at the interface is so high that it either leaves no more available electronic states for photo-excited carriers or it exceeds the density of photogenerated carriers [32]. The ratio photoconductivity/dark conductivity (P/D) of the LAO/STO thin films (Fig. 2(d)) supports this scenario. The conductivity of STO in the 2DEG state (LAO/STO #4) is barely changed under illumination. However, for the insulating sample LAO/STO #1, the photo-induced carriers are ruling the carrier density of the system, remarkably enhancing the conductivity.

C. Photo-controlled conductive interface

After having shown the symmetry-breaking nature of the oxide-STO system, we now investigate the conductivity of the interface as it is well known that the carrier mobility of $SrTiO_3$ is very high at low temperatures. The interface of oxide-$SrTiO_3$ shall in principle inherit this property and exhibit high conductivity or even metallic behavior. To verify this, we conducted the polarization vs electric field measurements for an epitaxial $BiFeO_3$ (BFO) thin film deposited on STO (BFO/STO). If the interface is highly conductive, it will behave like a bottom metal underneath the oxide allowing BFO polarization to switch upon an external bias voltage applied to the top electrodes (see Fig. 3(d)).

Ferroelectric hysteresis vs electric field (P-V) loops and current vs electric (I-V) measurement of BFO/STO monodomain thin films were recorded using an aixACCT TF3000 ferroelectric workstation under simultaneous illumination with the 405 nm monochromatic light. The polarization (Fig. (a)) and current (Fig. 3(b)) vs applied voltage at 10 K reveal either dielectric or ferroelectric behavior depending on illumination conditions. Classic dielectric behavior is seen in dark and under low-intensity illumination. Clear current peaks associated with polarization switching are seen under high laser intensity illumination, indicating partial switching of ferroelectric polarization at the coercive voltage V_c of ~4 V to ~6 V. The light intensity dependence of V_c, i.e., the coercive voltage decreases with increasing laser intensity (Fig. 3(c)), evidences the facile control of ferroelectricity via in-plane geometric electrodes.

We noticed that the ferroelectric polarization (~8 μC/cm^2) at 10 K is about 10 % of the expected value of BFO thin films. This is probably due to a partial polarization switching BFO (Fig. 3(d)). Only a limited amount of photocarriers may diffuse underneath the top metal electrode to screen the polarization while switching. As the temperature approaches 40 K, the electron mobility of STO dramatically drops and switching cannot be performed. (Fig. 3(e) and 3(f)).

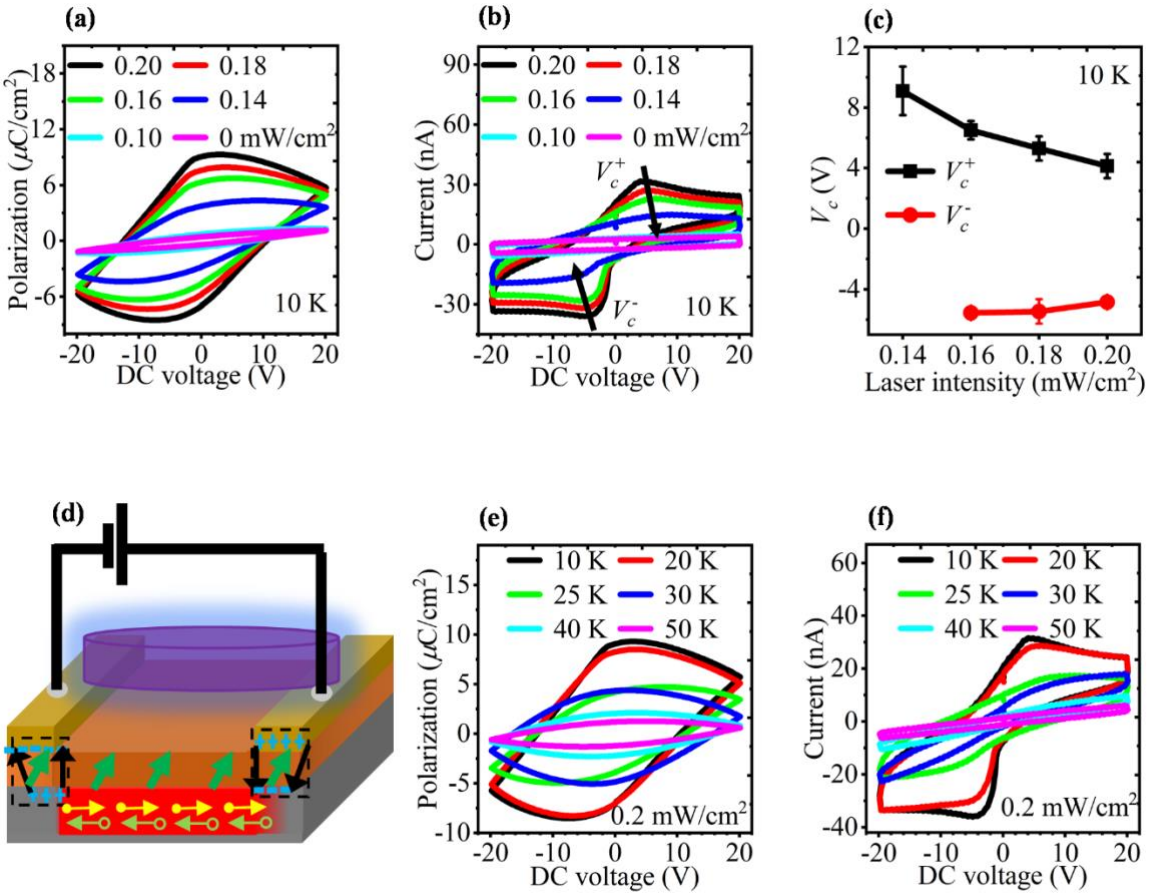

FIG. 3. Ferroelectric *P-V* hysteresis loop of BFO/STO thin film under illumination. Laser intensity-dependent (a) *P-V* loops, (b) *I-V* curves and (c) the coercive voltage at 10 K. (d) Schematic illustration of *P-V* loops measurement. yellow solid dots and light green open circles represent electrons and holes, respectively, their corresponding arrows indicate the moving directions upon an applied DC voltage. Black arrows indicate the electric field across the thin film. Green arrows indicate the ferroelectric polarization of the thin film. The black-dash square boxes indicate the polarization in operation. Temperature-dependent (e) *P-V* loops and (f) *I-V* curves were measured under illumination at the laser intensity of 0.2 mW/cm^2.

IV. CONCLUSION

The aforementioned experiments and analysis show that interfaces of STO with different oxides such as Fe_2O_3 and LAO are generating a built-in electric field and polar state in STO including in the quantum paraelectric phase. The above effects might be a more general property of STO interface with classical oxides where the internal electrostatic potential is about a few hundred meV, corresponding to an electric field beneath the STO surface of about 1 mV/nm [33,34]. Such a high interface built-in field might be able to induce a quantum ferroelectric state according to the electric field-temperature phase diagram [35]. (see Fig. 5 in Appendix B)

In contrast to the 2DEG interface which undergoes a significant electronic reconstruction, the insulting interface with less initially trapped carriers during sample growth is more prone to a

polar state. Nevertheless, even in the insulating state, the oxide-STO interface can still be conductive if sufficient free electrons such as photocarriers generated under illumination are provided [36]. Therefore, the photoconductive interface bridges the capping layer and STO substrate and largely extends the multifunctional degrees of freedom, e.g. spin-charge conversion as recently highlighted [37]. Our work not only shows that a bulk photovoltaic effect can be used to detect the symmetry breaking of media but also presents that STO-based heterostructures are promising for designing multi-functional devices.

ACKNOWLEDGEMENTS

The work was partly supported by the EPSRC (UK) through grants no. EP/T027207/1 and EP/P025803/1. H. Z. acknowledges the Warwick-China Scholarships and China Scholarship Council. The authors acknowledge Dorin Rusu and Adam Cooper for the fruitful discussion on the sample growth. The authors also deeply acknowledge MingMin Yang for helping design the PPMS optical insert.

APPENDIX

A. Linear bulk photovoltaic current measurements

Photocurrents as a function of the HWP angle were individually measured at different temperatures to determine the polarity of the structure. Linear bulk photovoltaic currents for Au/STO, Al/STO, Fe_2O_3/STO and LAO/STO are given in Fig. 4. Clearly, Au/STO and LAO/STO #1 at both high and low temperatures show classical bulk photovoltaic effect. on the contrary, Al/STO does not show any bulk photovoltaic effect at both high and low temperatures. The sample Fe_2O_3/STO does not show a bulk photovoltaic effect at room temperature, however, shows the bulk photovoltaic effect behavior at 10 K.

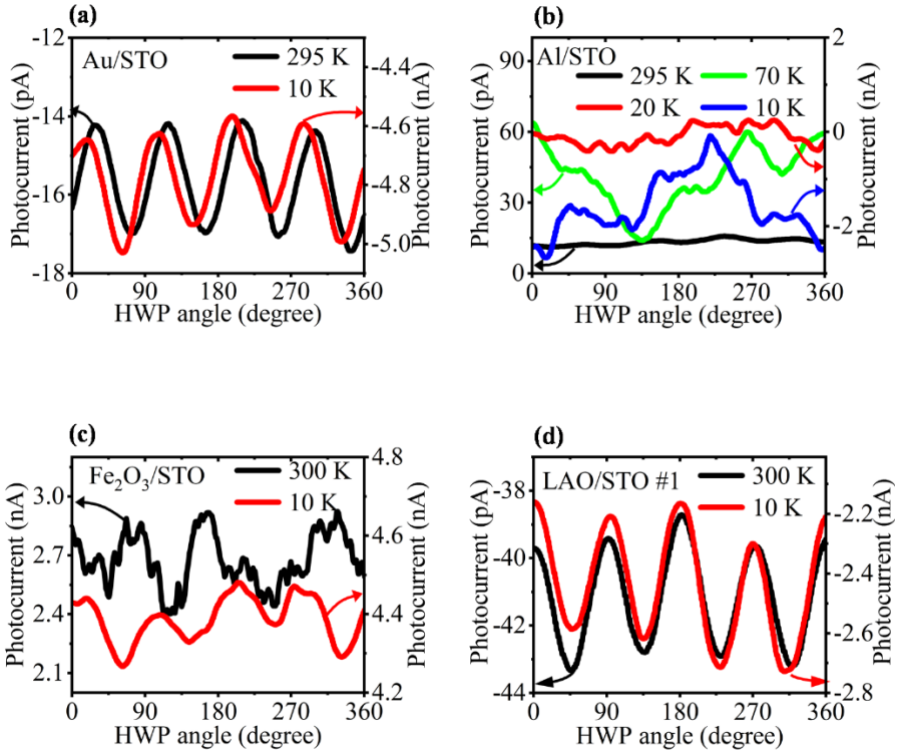

FIG. 4. Half-wave plate (HWP) angle-dependent photocurrents of (a) Au/STO, (b) Al/STO, (c) Fe_2O_3/STO and (d) LAO/STO #1 at different temperatures.

B. Electric field-temperature phase diagram of STO

To further understand why the bulk photovoltaic effect becomes stronger when the temperature is lowered in the quantum paraelectric phase of STO, we employed the phase diagram of STO as shown in Fig. 5[35]. As is known, when the temperature is decreased in the quantum paraelectric phase, STO approaches the virtual Curie temperature (below 0 K) [8,9]. This indicates that (a) an electrical field to induce a polar structure in STO is less needed; (b) a fixed

electrical field can induce stronger polarity. Though we cannot verify if this interface enters a ferroelectric state more than a polar state, the phase diagram still applies to our above analysis for a normal polar state.

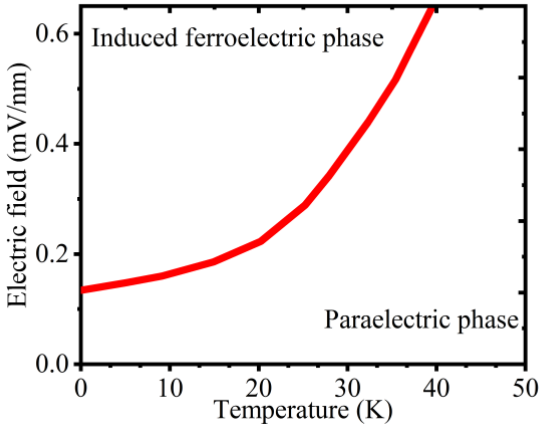

FIG. 5. Electric field-temperature phase diagram of STO [35].

C. Photocurrent vs Laser spot position

To prove that the photocurrent is not due to the injection of carriers from electrodes but purely due to the bulk photovoltaic effect generated by the polar LAO/STO interface, we have conducted further experiments using an optical cryostat (Attodry800) at both room temperature, of which the detail is given below, and low temperature. A pair of Au-Al electrodes (spacing 500 μm) were fabricated on the top of the LAO/STO #1 sample as shown in Fig. 6a. The photocurrent was measured by shifting the laser spot (about 150 μm radius) from the Al electrode to the Au electrode. It is addressed that due to the nature of the BPV effect, which allows the carriers diffuse over a certain distance, the photocurrent can be collected even if the laser spot is smaller than the distance between the electrodes [38]. The results in Fig. 6b and Fig. 6c-6e clearly show that the photocurrent has the maximum value when the laser spot was in the middle of the electrode pair. It can be easily seen the illumination is either on the Au or Al electrodes, the photocurrent is negligible. This directly proves that the photocurrent is not due to the injection of the electrode but due to a proper internal photoelectric effect within the LAO/STO region. It is worth noting that the photocurrent flow is due to the bulk photovoltaic effect, which is anisotropic due to the symmetry properties of crystals or the structures (determined by the BPV tensor [19]). Therefore, the measured current in our experiments represents the in-plane component of the three-dimensional BPV current.

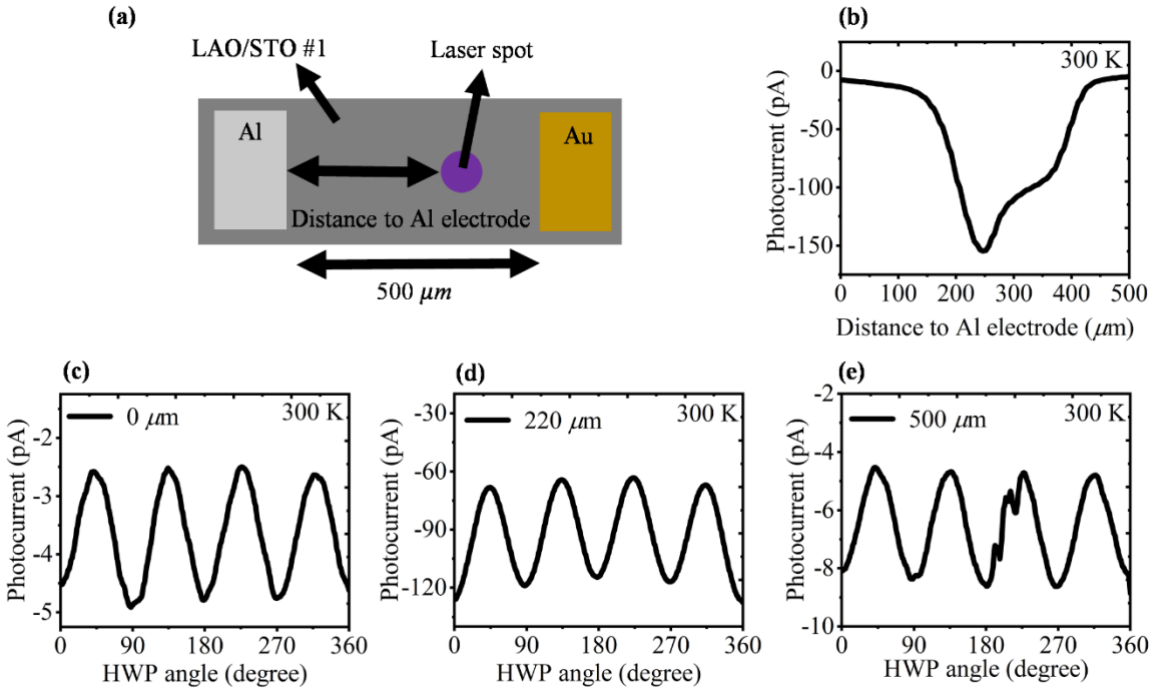

FIG. 6. Laser spot-dependent photocurrent measurement. (a) Experimental setup. Al and Au electrode pair with a spacing of 500 μm was fabricated on the LAO/STO #1 sample. The laser spot was moved from the Al electrode to the Au electrode. (b) The photocurrent as a function of the laser spot position at 300 K. (c)-(e) The bulk photovoltaic currents measured at different laser spot positions at 300 K. The glitch in (e) is due to the noise signal.

References

[1] E. Sawaguchi and A. Kikuchi, Dielectric constant of strontium titanate at low temperatures. J. Phys. Soc. Jpn. **17**, 1666 (1962).

[2] K. A. Müller and H. Burkard, $SrTiO_3$: an intrinsic quantum paraelectric below 4 K. Phys. Rev. B **19**, 3593 (1979).

[3] A. Ohtomo and H. Y. Hwang, A high-mobility electron gas at the $LaAlO_3/SrTiO_3$ heterointerface. Nature **427**, 423 (2004).

[4] S. Thiel, G. Hammerl, A. Schmehl, C. W. Schneider, and J. Mannhart, Tunable quasi-two-dimensional electron gases in oxide heterostructures. Science **313**, 1942 (2006).

[5] J. A. Bert, B. Kalisky, C. Bell, M. Kim, Y. Hikita, H. Y. Hwang, and K. A. Moler, Direct imaging of the coexistence of ferromagnetism and superconductivity at the $LaAlO_3/SrTiO_3$ interface. Nat. Phys. **7**, 767 (2011).

[6] N. Reyren, S. Thiel, A. D. Caviglia, L. F. Kourkoutis, G. Hammerl, C. Richter, C. W. Schneider, T. Kopp, A. S. Ruetschi, D. Jaccard, *et al.*, Superconducting interfaces between insulating oxides. Science **317**, 1196 (2007).

[7] O. Tufte and P. Chapman, Electron mobility in semiconducting strontium titanate. Phys. Rev. **155**, 796 (1967).

[8] K. A. Muller, W. Berlinger, and E. Tosatti, Indication for a novel phase in the quantum paraelectric regime of $SrTiO_3$. Zeitschrift Fur Physik B-Condensed Matter **84**, 277 (1991).

[9] J. Hemberger, M. Nicklas, R. Viana, P. Lunkenheimer, A. Loidl, and R. Bohmer, Quantum paraelectric and induced ferroelectric states in $SrTiO_3$. J. Phys.-Condes. Matter **8**, 4673 (1996).

[10] M. Itoh, R. Wang, Y. Inaguma, T. Yamaguchi, Y. J. Shan, and T. Nakamura, Ferroelectricity induced by oxygen isotope exchange in strontium titanate perovskite. Phys. Rev. Lett. **82**, 3540 (1999).

[11] J. G. Bednorz and K. A. Muller, $Sr_{1-x}Ca_xTiO_3$: an XY quantum ferroelectric with transition to randomness. Phys. Rev. Lett. **52**, 2289 (1984).

[12] C. W. Rischau, X. Lin, C. P. Grams, D. Finck, S. Harms, J. Engelmayer, T. Lorenz, Y. Gallais, B. Fauque, J. Hemberger, *et al.*, A ferroelectric quantum phase transition inside the superconducting dome of $Sr_{1-x}Ca_xTiO_3$-delta. Nat. Phys. **13**, 643 (2017).

[13] L. Li, C. Richter, J. Mannhart, and R. C. Ashoori, Coexistence of magnetic order and two-dimensional superconductivity at $LaAlO_3/SrTiO_3$ interfaces. Nat. Phys. **7**, 762 (2011).

[14] H. Y. Hwang, Y. Iwasa, M. Kawasaki, B. Keimer, N. Nagaosa, and Y. Tokura, Emergent phenomena at oxide interfaces. Nat. Mater. **11**, 103 (2012).

[15] M. M. Yang, Z. D. Luo, Z. Mi, J. J. Zhao, E. S. Pei, and M. Alexe, Piezoelectric and pyroelectric effects induced by interface polar symmetry. Nature **584**, 377 (2020).

[16] D. H. Choe, D. West, and S. B. Zhang, Band alignment and the built-in potential of solids. Phys. Rev. Lett. **121**, 196802 (2018).

[17] A. Klein, Energy band alignment at interfaces of semiconducting oxides: A review of experimental determination using photoelectron spectroscopy and comparison with theoretical predictions by the electron affinity rule, charge neutrality levels, and the common anion rule. Thin Solid Films **520**, 3721 (2012).

[18] Y. G. Shi, Y. F. Guo, X. Wang, A. J. Princep, D. Khalyavin, P. Manuel, Y. Michiue, A. Sato, K. Tsuda, S. Yu, *et al.*, A ferroelectric-like structural transition in a metal. Nat. Mater. **12**, 1024 (2013).

[19] V. I. Belinicher and B. I. Sturman, The photogalvanic effect in media lacking a center of symmetry. Sov. Phys. Usp **23**, 199 (1980).

[20] B. I. Sturman and V. M. Fridkin, *The Photovoltaic and Photorefractive Effects in Noncentrosymmetric Materials* (Gordon and Breach Science Publishers, Philadelphia, 1992).

[21] A. Bhatnagar, A. R. Chaudhuri, Y. H. Kim, D. Hesse, and M. Alexe, Role of domain walls in the abnormal photovoltaic effect in $BiFeO_3$. Nat. Commun. **4**, 8 (2013).
[22] D. S. Knoche, M. Steimecke, Y. Yun, L. Muhlenbein, and A. Bhatnagar, Anomalous circular bulk photovoltaic effect in $BiFeO_3$ thin films with stripe-domain pattern. Nat. Commun. **12**, 282 (2021).
[23] J. Mannhart and D. G. Schlom, Oxide interfaces-an opportunity for electronics. Science **327**, 1607 (2010).
[24] D. A. Dikin, M. Mehta, C. W. Bark, C. M. Folkman, C. B. Eom, and V. Chandrasekhar, Coexistence of superconductivity and ferromagnetism in two dimensions. Phys. Rev. Lett. **107**, 056802 (2011).
[25] S. W. Zeng, X. M. Yin, T. S. Herng, K. Han, Z. Huang, L. C. Zhang, C. J. Li, W. X. Zhou, D. Y. Wan, P. Yang, *et al.*, Oxygen electromigration and energy band reconstruction induced by electrolyte field effect at oxide interfaces. Phys. Rev. Lett. **121**, 146802 (2018).
[26] G. Berner, A. Muller, F. Pfaff, J. Walde, C. Richter, J. Mannhart, S. Thiess, A. Gloskovskii, W. Drube, M. Sing, *et al.*, Band alignment in $LaAlO_3/SrTiO_3$ oxide heterostructures inferred from hard x-ray photoelectron spectroscopy. Phys. Rev. B **88**, 115111 (2013).
[27] Z. C. Zhong, P. X. Xu, and P. J. Kelly, Polarity-induced oxygen vacancies at $LaAlO_3/SrTiO_3$ interfaces. Phys. Rev. B **82**, 165127 (2010).
[28] Y. Li, S. N. Phattalung, S. Limpijumnong, J. Kim, and J. Yu, Formation of oxygen vacancies and charge carriers induced in the n-type interface of a $LaAlO_3$ overlayer on $SrTiO_3$(001). Phys. Rev. B **84**, 245307 (2011).
[29] A. Kalabukhov, R. Gunnarsson, J. Borjesson, E. Olsson, T. Claeson, and D. Winkler, Effect of oxygen vacancies in the $SrTiO_3$ substrate on the electrical properties of the $LaAlO_3/SrTiO_3$ interface. Phys. Rev. B **75**, 121404(R) (2007).
[30] A. Fete, C. Cancellieri, D. Li, D. Stornaiuolo, A. D. Caviglia, S. Gariglio, and J. M. Triscone, Growth-induced electron mobility enhancement at the $LaAlO_3/SrTiO_3$ interface. Appl. Phys. Lett. **106**, 051604 (2015).
[31] G. Herranz, M. Basletic, M. Bibes, C. Carretero, E. Tafra, E. Jacquet, K. Bouzehouane, C. Deranlot, A. Hamzic, J. M. Broto, *et al.*, High mobility in $LaAlO_3/SrTiO_3$ heterostructures: Origin, dimensionality, and perspectives. Phys. Rev. Lett. **98**, 216803 (2007).
[32] S. A. Chambers, M. H. Engelhard, V. Shutthanandan, Z. Zhu, T. C. Droubay, L. Qiao, P. V. Sushko, T. Feng, H. D. Lee, T. Gustafsson, *et al.*, Instability, intermixing and electronic structure at the epitaxial $LaAlO_3/SrTiO_3$(001) heterojunction. Surface Science Reports **65**, 317 (2010).
[33] S. A. Chambers, L. Qiao, T. C. Droubay, T. C. Kaspar, B. W. Arey, and P. V. Sushko, Band alignment, built-in potential, and the absence of conductivity at the $LaCrO_3/SrTiO_3$(001) Heterojunction. Phys. Rev. Lett. **107**, 206802 (2011).
[34] P. Schutz, F. Pfaff, P. Scheiderer, Y. Z. Chen, N. Pryds, M. Gorgoi, M. Sing, and R. Claessen, Band bending and alignment at the spinel/perovskite gamma-$Al_2O_3/SrTiO_3$ heterointerface. Phys. Rev. B **91**, 165118 (2015).
[35] J. Hemberger, P. Lunkenheimer, R. Viana, R. Bohmer, and A. Loidl, Electric-field-dependent dielectric constant and nonlinear susceptibility in $SrTiO_3$. Phys. Rev. B **52**, 13159 (1995).
[36] H. B. Zhang and M. Alexe, Optoelectronic functionality of $BiFeO_3$-$SrTiO_3$ interface. Adv. Electron. Mater. **8**, 2100665 (2022).
[37] P. Noel, F. Trier, L. V. M. Arche, J. Brehin, D. C. Vaz, V. Garcia, S. Fusil, A. Barthelemy, L. Vila, M. Bibes, *et al.*, Non-volatile electric control of spin-charge conversion in a $SrTiO_3$ Rashba system. Nature **580**, 483 (2020).

[38] Y. Heo, H. B. Zhang, and M. Alexe, Dynamic control of piezoelectricity enhancement via modulation of the bulk photovoltaic effect in a $BiFeO_3$ thin film. Adv. Electron. Mater. **8** (2022).